Int. J. Solids Structures Vol. 21, No. 4, pp. 389–397, 1985
Printed in the U.S.A.

0020–7683/85 $3.00 + .00

THE ORIGIN OF SPURIOUS RESONANCES IN COMPOSITE RESONATORS

K. B. Yoo and H. Überall
Physics Department, Catholic University, Washington, D.C. 20064, U.S.A.

(*Received* 21 *November* 1983; *in revised form* 15 *June* 1984)

Abstract—Three-dimensional models have been developed to explain the characteristics of composite resonators. Simple disc or rectangular plate models predict resonance frequencies that are in excellent agreement with the results of experimental measurement. In particular, agreement with the relatively complicated spurious resonance frequency spectra is remarkable, whereas a standard one-dimensional model lacks this feature. The geometry of the resonator is found to be directly responsible for the spurious resonances as well as the principal resonances. It is suggested that a way of eliminating or at least controlling the unwanted modes can be found since the origin of the spurious frequencies is now understood.

1. INTRODUCTION

Recent technological developments[1–4] have made it possible to fabricate a bulk acoustic wave resonator on a silicon substrate with fundamental frequency in the very high/ultrahigh frequency range. The theoretical analysis of the device, however, has been limited to a one-dimensional model[1–4]. Although this model can reasonably predict certain resonance frequencies, it fails to include observed spurious resonance frequencies that are presenting some problems in achieving good resonators or filters. The present work is intended to improve the simple model. Three-dimensional models have been developed with the aim of understanding why the spurious resonances occur and how they can be controlled.

The composite resonator[1–4] consists of a thin silicon membrane etched out of a block of silicon to a thickness of a few microns and a sputter-deposited piezoelectric ZnO film of comparable thickness. At the top and bottom of the piezoelectric film, there are located thin electrode layers to excite the resonator. A typical resonator has a circular top electrode with an area smaller than that of the silicon diaphragm. The first model we thus consider is naturally a circular disc model to represent the actual vibrating region. As the result of satisfying boundary conditions on the surfaces, we get a characteristic frequency equation. The calculated spectrum of frequencies clearly shows principal frequencies as well as overtones (spurious frequencies).

The principal frequencies are generated by satisfying boundary conditions in the axial direction, as in the one-dimensional model. Finite size in the radial direction causes the spurious frequencies. Comparison with results of an experimental measurement of a filter with rectangular top electrodes shows rather good agreement[5]. The spacings between spurious frequencies are well predicted by this model, although the disc is not exactly suited to represent the rectangular electrode resonator.

To accurately represent the vibrating region, a rectangular plate model was tried to see if our results could be improved. Indeed, most of the spurious resonance peaks are predicted with this model, and overall agreement is excellent. Considering the simplicity of these models, the accuracy of our frequency predictions is remarkable. These models thus constitute a very useful tool for understanding the complicated resonance structure of the composite resonator.

Together with the information provided by the associated mode functions, it now appears possible to suppress unwanted modes while reinforcing a selected mode. These models are now being extended to two-layer coupled discs or rectangular plates so that complete information on the resonators can be obtained[6].

2. THREE-DIMENSIONAL MODELS

2.1 *Disc model*

The composite resonator is first modeled as a single, homogeneous, isotropic elastic disc of radius a and thickness $2L$. (It should be mentioned, however, that ZnO and Si are not isotropic.) On the flat top and bottom surfaces, free boundary conditions are assumed, with the vanishing of all stresses ($\tau_{zz} = \tau_{zr} = \tau_{z\theta} = 0$).

On the curved edge surface, the conditions for a free boundary are the vanishing of all stresses ($\tau_{rr} = \tau_{r\theta} = \tau_{rz} = 0$), or for a clamped boundary the vanishing of particle displacements ($u_r = u_\theta = u_z = 0$). It is, however, well known that in the elastodynamic problem of finite bodies, not all boundary conditions can be simultaneously satisfied. We thus follow the approach of Aggarwal[7] to satisfy the maximum number of boundary conditions. Specifically, for the azimuthally symmetric problem at hand, we first satisfy the relevant free boundary conditions at $z = \pm L$, namely,

$$\tau_{zz} = \tau_{zr} = 0. \tag{1}$$

On the curved boundary, only one of the two conditions ($\tau_{rr} = \tau_{rz} = 0$ for a free or $u_r = u_z = 0$ for a clamped boundary) can then be satisfied at a time. With the geometry of the resonator under consideration (radius $a \sim 100L$), it appears that the choice of any of these conditions will influence the results very little; this is indeed found to be the case[5].

Introducing potentials by

$$\mathbf{u} = \nabla\phi + \nabla \times \boldsymbol{\psi} \tag{2}$$

where $\psi_z = \psi_r = 0$, and with a time factor $\exp(-i\omega t)$ suppressed, the solutions of the appropriate wave equations symmetric about $z = 0$ are

$$\phi = AJ_0(pr) \cos K_h z \tag{3a}$$

$$\psi_\theta = DJ_1(pr) \sin K_k z, \tag{3b}$$

where

$$K_h^2 = h^2 - p^2 \tag{4a}$$

$$K_k^2 = k^2 - p^2 \tag{4b}$$

and

$$h = \frac{\omega}{c_L} \tag{5a}$$

$$k = \frac{\omega}{c_T}, \tag{5b}$$

c_L and c_T being longitudinal and transverse wave speeds, respectively, in the disc. If now eqn (1) is satisfied and A and D eliminated, one obtains the characteristic equation of the problem,

$$\frac{\tan K_k L}{\tan K_h L} = -\frac{4p^2 K_h K_k}{(p^2 - K_k^2)^2}, \tag{6}$$

which couples longitudinal and transverse modes. The remaining parameter p is determined from one of the two boundary conditions at $r = a$.

Satisfying $\tau_{rz} = 0$ or $u_r = 0$ leads to

$$J_1(pa) = 0; \tag{7a}$$

satisfying $\tau_{rr} = 0$ gives

$$J_0(pa) = (1 - \nu)\frac{J_1(pa)}{pa}, \tag{7b}$$

where ν is Poisson's ratio; and satisfying $u_z = 0$ gives

$$J_0(pa) = 0. \tag{7c}$$

2.2 *Rectangular plate model*

For the composite resonators with rectangular electrodes, this model will be better suited than the disc model. As in the disc model, the single, homogeneous, isotropic elastic plate is assumed to have side lengths $2a$ and $2b$ with thickness $2L$. The displacement vector $\mathbf{u}$ can be expressed[8] in terms of a scalar potential ϕ and a partial displacement $\mathbf{u}'$:

$$\mathbf{u} = \nabla\phi + \mathbf{u}' \tag{8a}$$

with

$$\nabla \cdot \mathbf{u}' = 0. \tag{8b}$$

Considering only symmetric displacements with respect to the $z = 0$ plane, we have

$$u_x = -A \sin k_1x \cos k_2y \cos k_3z + B_1 \sin q_1x \cos q_2y \cos q_3z \tag{9a}$$

$$u_y = -A\frac{k_2}{k_1} \cos k_1x \sin k_2y \cos k_3z + B_2 \cos q_1x \sin q_2y \cos q_3z \tag{9b}$$

$$u_z = -A\frac{k_3}{k_1} \cos k_1x \cos k_2y \sin k_3z + B_3 \cos q_1x \cos q_2y \sin q_3z, \tag{9c}$$

where

$$k_3^2 = h^2 - (k_1^2 + k_2^2) \tag{10a}$$

$$q_3^2 = k^2 - (q_1^2 + q_2^2). \tag{10b}$$

To satisfy the stressfree condition on the $z = \pm L$ surfaces for all x and y, q_1 has to be equal to k_1 and q_2 equal to k_2. Then we obtain the characteristic equation for this case:

$$\frac{\tan q_3L}{\tan k_3L} = -\frac{4q_3k_3(k_1^2 + k_2^2)}{(k_1^2 + k_2^2 - q_3^2)^2}. \tag{11}$$

Here, k_1 and k_2 are determined from the boundary conditions on $x = \pm a$ and $y = \pm b$, respectively.

Satisfying $\tau_{xx} = 0$ or $u_y = u_z = 0$ at $x = \pm a$ leads to

$$k_1 = \frac{2m + 1}{2a}\pi; \tag{12a}$$

satisfying $\tau_{zx} = \tau_{xy} = 0$ or $u_x = 0$ leads to

$$k_1 = \frac{m}{a}\pi. \tag{12b}$$

We obtain similar equations for k_2 by satisfying boundary conditions at $y = \pm b$:

$$k_2 = \frac{2n + 1}{2b}\pi \tag{13a}$$

or

$$k_2 = \frac{n}{b}\pi, \tag{13b}$$

where m and n are integers.

Since the frequency equation depends only on $k_1^2 + k_2^2$, we can summarize the conditions as follows: for $\tau_{xx} = \tau_{yy} = 0$,

$$k_1^2 + k_2^2 = \left[\left(\frac{2m + 1}{2a}\right)^2 + \left(\frac{2n + 1}{2b}\right)^2\right]\pi^2, \tag{14a}$$

and for $\tau_{zx} = \tau_{xy} = \tau_{yz} = 0$,

$$k_1^2 + k_2^2 = \left[\left(\frac{m}{a}\right)^2 + \left(\frac{n}{b}\right)^2\right]\pi^2. \tag{14b}$$

As in the disc model, these boundary conditions are expected to affect the resulting resonance frequencies very little.

3. RESULTS AND DISCUSSIONS

To compare the effects of radial boundary conditions on the resonance frequencies, a single ZnO disc with $a = 380$ μm and $L = 3.5$ μm was considered. The acoustic velocities used were those of ZnO: $c_L = 6370$ m/sec and $c_T = 2735$ m/sec.

Figure 1 shows the results of three different boundary conditions at $r = a$: $\tau_{rr} = 0$ (top), $u_z = 0$ (center) and $\tau_{rz} = 0$ or $u_r = 0$ (bottom). Two lowest principal frequencies that are trailed by sets of spurious frequencies appear in this figure. As expected (see above), different boundary conditions lead to very similar results for the reasons stated. Although not shown, an analogous behavior was obtained for the rectangular plate model. Here the amplitudes were taken arbitrarily, guided only by the fact that the higher-order modes get successively less excited. The principal frequencies are obtained by satisfying boundary conditions on the z-surfaces, eqn (6), with the lowest-order solution p of eqn (7). Higher-order solutions of eqn (7) give rise to spurious resonance frequencies for a given principal frequency. At the fundamental frequency, the spurious frequencies trail off toward the lower (left) frequency side, but the trend reverses at the first overtone frequency. This general behavior can easily be recognized by inspecting dispersion curves, which will be discussed later in this section.

Being assured now that the boundary condition at $r = a$ does not cause any significant differences in the frequency spectrum, we next examine, in Fig. 2, the effect of reducing the disc radius from $a = 380$ μm successively down to $a/2$, $a/4$ and $a/6$ for the case of $\tau_{rz} = 0$. The successive increase in the spacing of the spurious resonances (with only a small accompanying shift in the position of the fundamental) is clearly visible here. A reversal of the end of the trail of spurious frequencies is noted in the case of $a/6$.

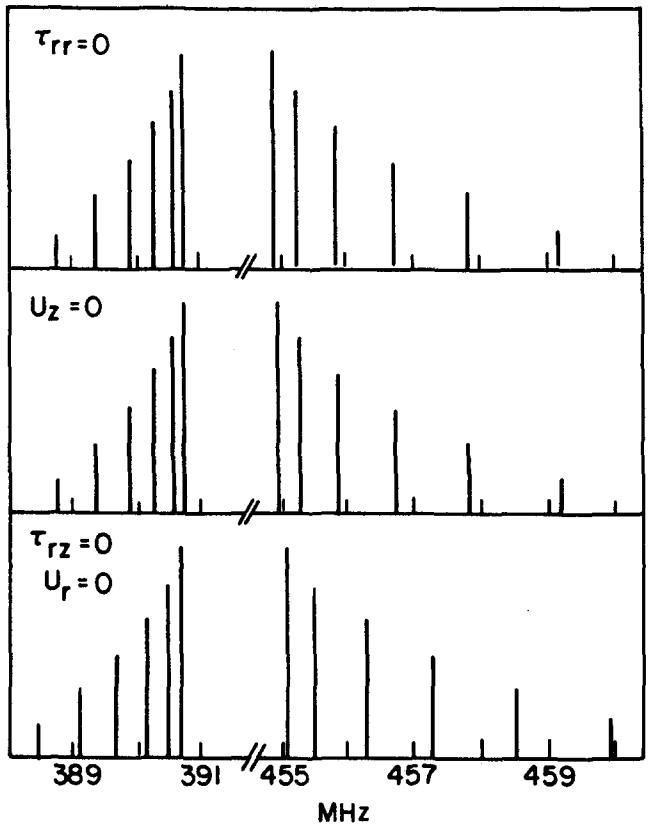

Fig. 1. Theoretical frequency spectra of a single circular ZnO disc (a = 380 μm, L = 3.5 μm) with boundary conditions at $r = a$: $\tau_{rr} = 0$ (top), $u_z = 0$ (center) and $\tau_{rz} = 0$ or $u_r = 0$ (bottom).

Figure 3a shows typical experimental results[9] in which the composite resonator was used as a part of a filter in the half-wavelength mode. One notices a fundamental resonance at 425 MHz, which is trailed toward the lower-frequency side by a series of smaller spurious resonances; there are further indications of a weak first overtone at ~445 MHz, which this time is trailed toward the high-frequency side by another series of spurious resonances. Much more distinct indications of the first overtone and its trail of resonances are provided by unpublished experimental work. An example of this is provided in Fig. 3d (courtesy of T. W. Grudkowski).

The filter corresponding to Fig. 3a had a silicon thickness of 5.6 μm, a ZnO thickness of 2.47 μm and rectangular top electrodes (254 × 508 μm) spaced 12 μm from each other. We first modeled the resonator part of the device by a disc of radius a = 250 μm of total thickness $2L$ = 8.1 μm. To take into account the composite nature of the device, longitudinal and transverse wave velocities were adjusted to the principal frequencies in the limit of infinite radial extent[10]. The effective velocities thus obtained were c_L = 7160 m/sec and c_T = 3443 m/sec, both lying inbetween the corresponding values for ZnO and Si. This leads to the frequency spectrum of Fig. 3b subject to the boundary condition $\tau_{rz} = 0$ at $r = a$.

The fit to the experimental spectrum of Fig. 3a is very good. Both the fundamental at 425 MHz as well as its sequence of five spurious resonances are reproduced fairly well. In addition, the experimental sequence of a first overtone at ~445 MHz and its three or more spurious resonances (all of feeble intensity owing to the weak coupling of these resonances in the filter) are also reproduced.

To make an improvement on the model, we next employed the rectangular plate model since the resonator had rectangular electrodes. In this way, the flat area of the model could be chosen to be exactly the same as that of the electrodes, and better agreement was expected. The effective velocities and thickness of the model were the same as in the disc. Figure 3c shows the prediction of this model. The number of

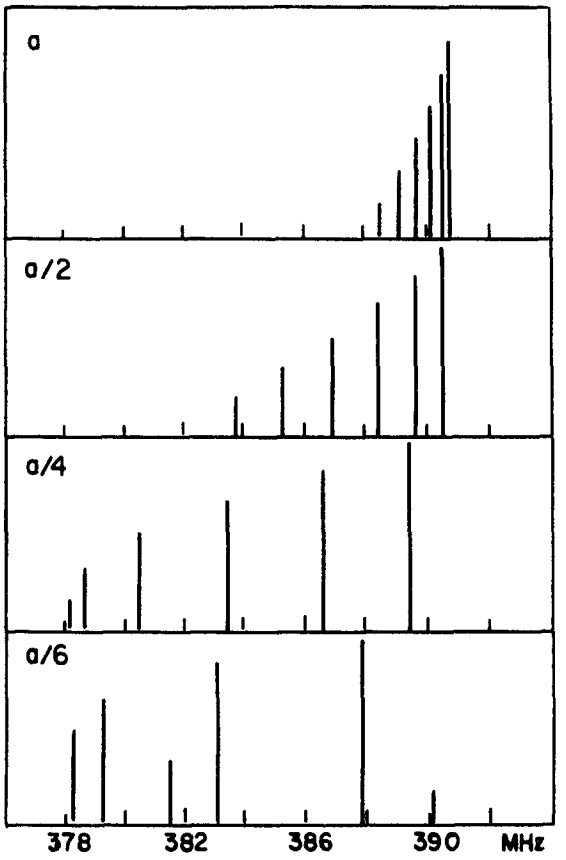

Fig. 2. Effect of a reduction in the disc radius on the spacing in the frequency spectrum. Successively from top: radius a = 380 μm corresponding to Fig. 1, radius $a/2$, $a/4$, $a/6$.

spurious frequencies increased considerably, but the agreement with the data of Fig. 3a is excellent. Not only do the major peaks coincide with the predictions, but also the smaller wiggles on the lower-frequency side are seen to agree with them. Considering the simplicity of the models, this appears remarkable. The models are thus capable of explaining all the essential physical features of the devices, enabling us to pinpoint design problems or else find a way of developing improved resonators.

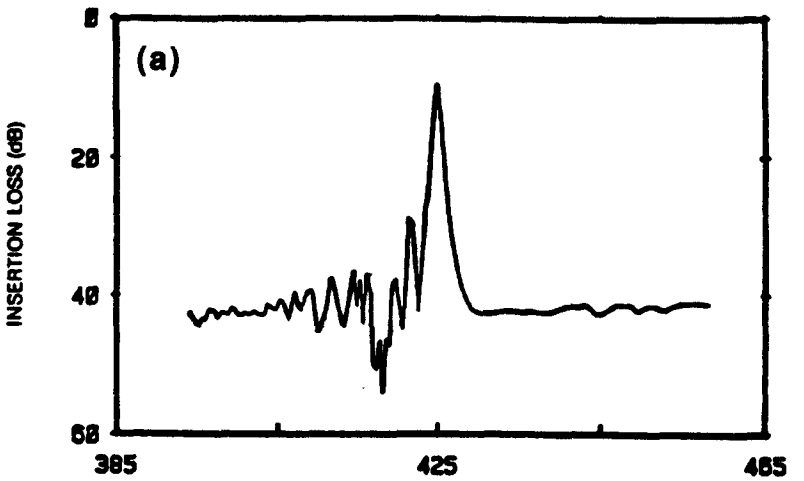

Fig. 3. (a) Experimental frequency spectrum of bulk-wave resonator (filter). (b) Theoretical frequency spectrum given by an effective single-disc resonator. (c) Theoretical frequency spectrum of an effective rectangular plate resonator. (d) Alternative experimental frequency spectrum corresponding to another comparable resonator (T. W. Grudkowski, unpublished).

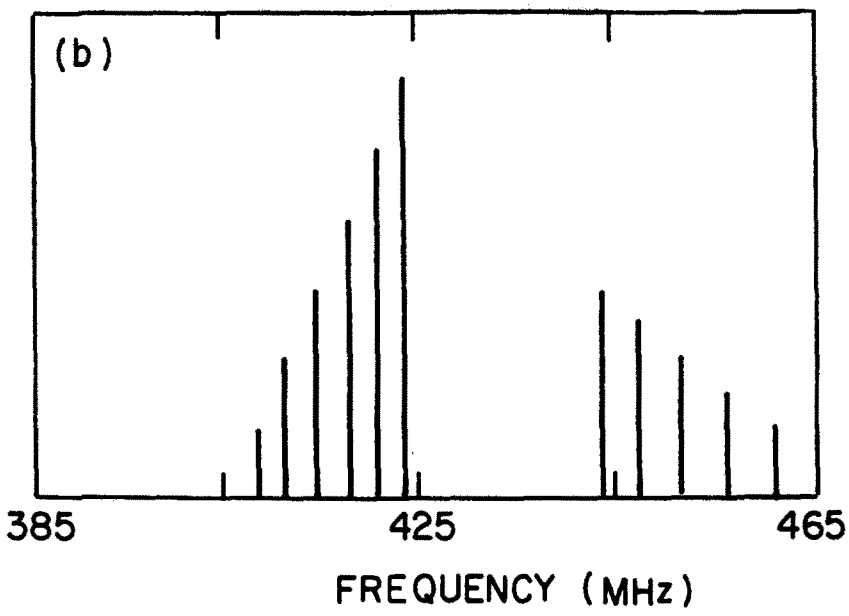

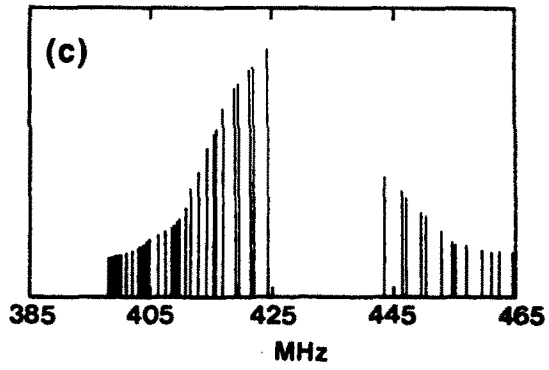

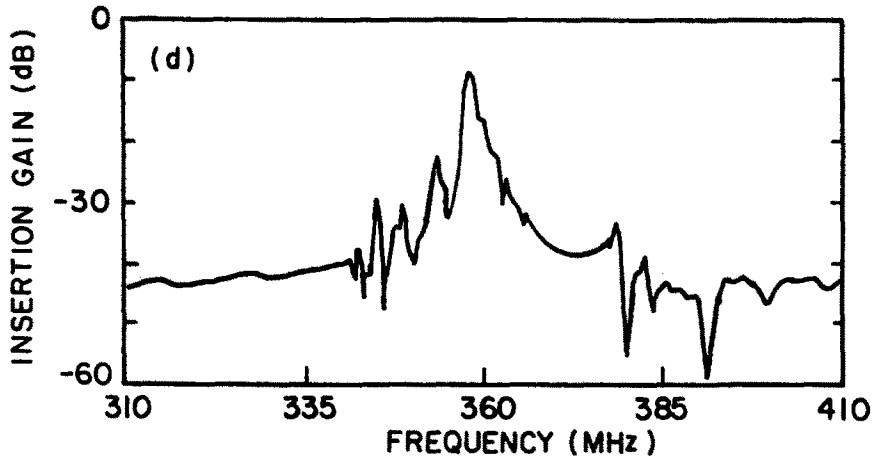

Fig. 3. (*Continued*)

It should be noted that, regarding finite-size resonators, more detailed calculations employing piezoelectric differential equations and anisotropic properties have appeared in the literature[11–13]. However, our simple models appear to explain all essential features of the experimental data, while providing us with a clearer picture of the relationship between frequencies and material parameters.

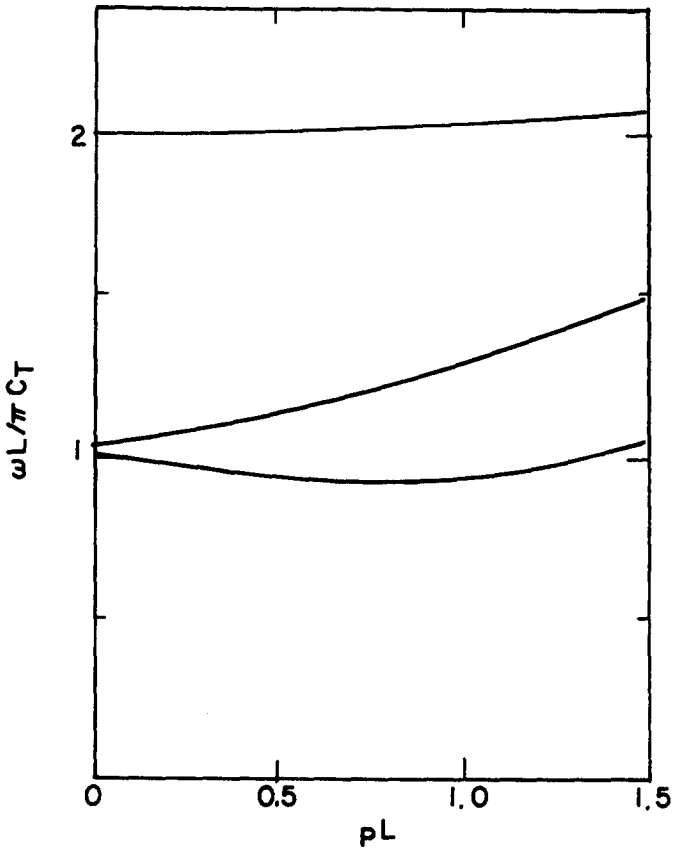

Fig. 4. Dispersion relations for the effective single resonator: c_L = 7160 m/sec, c_T = 3443 m/sec. Vertical axis shows dimensionless frequency $\omega L/\pi c_T$, and horizontal axis represents pL.

Dispersion curves for the modes are shown in Fig. 4. These are very useful in recognizing the qualitative behavior of a resonator. The lowest curve has negative slope initially and becomes positive when $pL \sim 0.75$. For the resonator analyzed here, $pL \ll 1$, and we see clearly from the curve that the spurious resonance frequencies will have lower frequencies than the fundamental since pL increases as we get to higher-order solutions of eqns (7) or (14). The next higher curve describes the behavior of the first overtone. It has positive slope throughout, and its spurious frequencies are expected to lie toward the higher-frequency side of the first overtone frequency. Indeed, the calculations and experimental measurement showed this clearly. Quantitatively, the slopes (or spacings between spurious frequencies) and the resonance frequencies naturally depend on the material property; transverse and longitudinal acoustic wave velocities are the material parameters that solely enter in this analysis.

In summary, the origin of spurious resonances has been clarified by the present approach, and with the understanding of the frequency spectra and mode functions of resonators gained hereby, it appears likely that the unwanted spurious modes can be removed, or their intensity controlled, by applying the information obtained from this modeling. Quantitative studies on this topic are now underway.

Acknowledgments—Support of this work by a U. S. government grant is acknowledged. Additional support was received from the Office of Naval Research.

REFERENCES

1. T. W. Grudkowski *et al. Proc. IEEE 1980 Ultrasonics Symposium*, p. 829 (1980).
2. T. W. Grudkowski, J. F. Black, G. W. Drake and D. E. Cullen, *Proc. 36th Annual Symposium on Frequency Control*, p. 537 (1982).
3. J. S. Wang, Ph.D. thesis, Dept. of Electrical Engineering, University of Southern California (1981).
4. K. M. Lakin and J. S. Wang, *Proc. IEEE 1980 Ultrasonics Symposium*, p. 834 (1980).

5. K. B. Yoo, H. Überall and W. Williams, Jr., *Proc. IEEE 1982 Ultrasonics Symposium*, p. 490 (1982).
6. K. B. Yoo, H. Überall, D. Ashrafi and S. Ashrafi, *Proc. 37th Annual Symposium on Frequency Control*, p. 317 (1983).
7. R. R. Aggarwal, *J. Acoust. Soc. Am.* **24**, 463 (1952).
8. R. W. Morse, *J. Acoust. Soc. Am.* **22**, 219 (1950).
9. T. W. Grudkowski *et al. Appl. Phys. Lett.* **37**, 993 (1980).
10. T. R. Meeker and A. M. Meitzler, in *Physical Acoustics, Vol. I* (Edited by W. P. Mason). Academic Press, New York (1964).
11. T. R. Meeker, *Proc. 31st. Annual Symposium on Frequency Control*, p. 35 (1977).
12. H. F. Tiersten and R. C. Smythe, *Proc. 31st Annual Symposium on Frequency Control*, p. 44 (1977).
13. W. P. Mason, *Piezoelectric Crystals and Their Application to Ultrasonics*, p. 93. D. Van Nostrand Co., New York (1950).